Earthquake Geotechnical Engineering, Ishihara (ed.) © 1995 Balkema, Rotterdam. ISBN 90 5410 578 X

Application of a dynamic effective stress model at a reclaimed site during the Great Hanshin earthquake, 1995

F.Yamazaki, M.A.Ansary & I.Towhata
University of Tokyo, Japan

ABSTRACT: Site response analyses were conducted at the Kobe Port Island site where surface and three downhole ground motions were recorded during the recent Great Hanshin earthquake. The analyses were conducted using a nonlinear dynamic effective stress method which took into account of the liquefaction under multi-directional shearing. The input motions were recorded directly at the base by the vertical array system. Computed and recorded ground motions and associated response spectra were in good agreement. Coupled effects of two horizontal motions on the dynamic response and liquefaction of the ground were also examined.

1 INTRODUCTION

The recent Great Hanshin earthquake in the vicinity of Kobe left many sites collapsed due to liquefaction. Most of the liquefaction occurred under the level ground condition[1]. Many researchers[2,3] showed that liquefaction is more liable to occur under multi-directional loading than under uni-directional loading and total stress method like SHAKE would underestimate the response at longer periods[4]. So, in this study the authors used multi-spring model[5,6] for effective stress dynamic response analysis of a liquefied site at the Kobe port area.

2 LOCATION AND SITE CONDITION

A one-dimensional vertical array is situated at the Kobe Port Island area, which is located 34.670° N and 135.208° E. The array is situated in a reclaimed land and consists of 4 three-component accelerometers. The location of the array is shown in Figure 1. From the borehole report, it can be summarized that upto a depth of 19 m is covered by fill (sandy gravel), it is followed by an alluvial clay deposit from 19 to 27 m. Next there is a diluvial soil layer composed of gravelly sand from 27 to 61 m, which is followed by a diluvial clay layer from 61 to 79 m. Below the clay layer there exists a gravelly sand layer. The water table is situated approximately at a depth of 4 m from the ground surface.

In this array site, orientation errors was detected from particle orbit plots of two horizontal components and were estimated by applying maximum coherence method[7] and maximum cross-correlation method[7]. The ground surface at this site was supposed to be liquefied, so accelerometer at GL-32 m was used as a reference

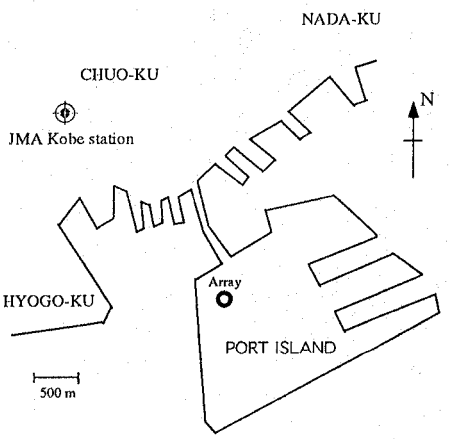

Fig. 1 Location of Port Island array and JMA station in Kobe

point instead of accelerometer at GL 0 m. In the orienatation error analysis β and γ angles were assumed to be zero and it was found from the single event record at hand that the accelerometer at GL-83 m may have an average orientation error of 19°. For further analysis for this study, corrected records were used.

3 COMPARISON OF RECORDS BETWEEN TWO SITES OF DIFFERENT SOIL CONDITIONS

Atfirst, the authors considered two sites of different soil conditions to show the effect of liquefaction on them. The first site is JMA's (Japan Meteorological Agency) Kobe station, which is a stiff soil site and the other is the site under consideration for this study,

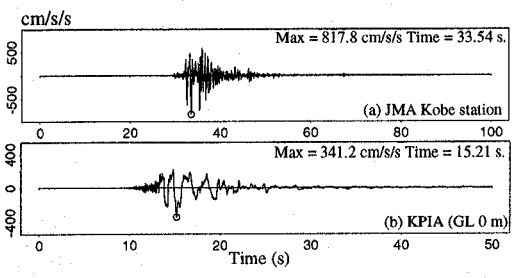

Fig.2 Recorded acceleration time histories of JMA Kobe station and of Kobe Port Island array (GL 0 m) for NS-component

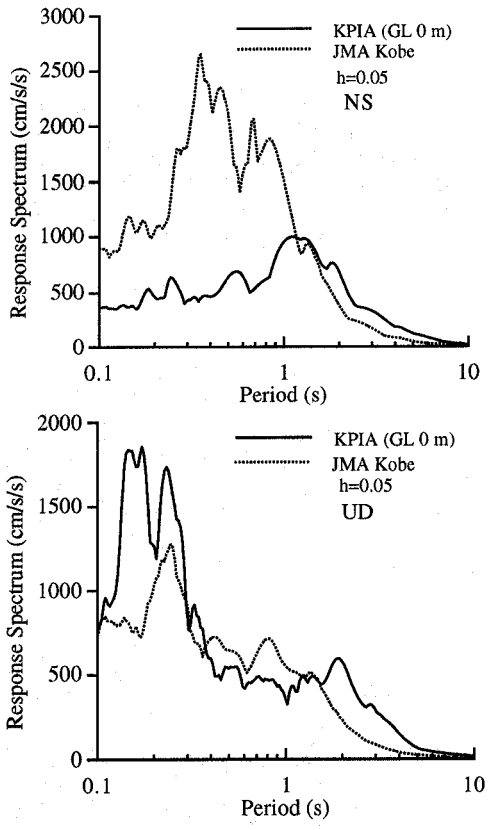

Fig.3 Comparison of acceleration response spectrum between JMA Kobe station and Port Island

which is a reclaimed land. The distance between these two sites is approximately 3 kilometers.

Figure 2 shows time histories of NS-component of both sites on the ground surface. It can be clearly seen from these figures that time history of stiff soil site has a higher frequency content than the other site. Figure 3 compares the response spectra between the two sites. The Kobe Port Island Array (KPIA) site has a longer-period motion than that of the JMA Kobe station for NS

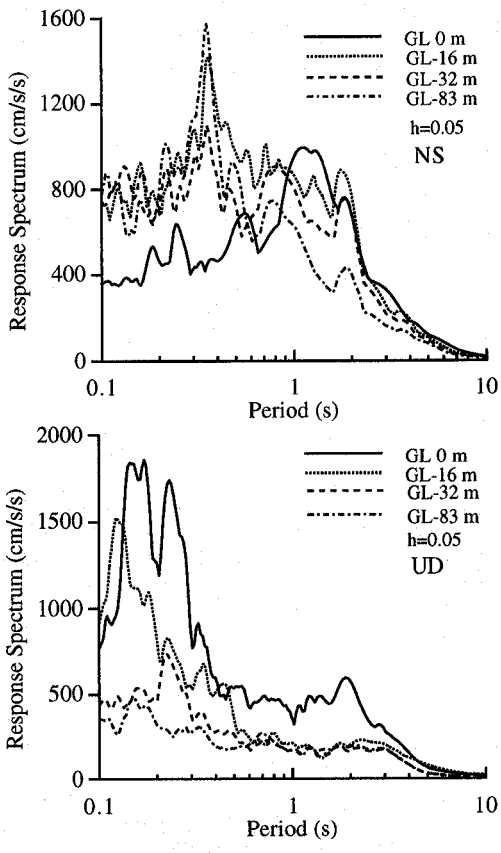

Fig.4 Comparison of acceleration response spectrum among different depths of Port Island vertical array

component. For the UD component, the sites have similar period content. The significant long period motion may be attributed to the occurrence of liquefaction in the reclaimed site. To investigate further, Figure 4 compares the response spectra for all the recorded NS and UD components of the vertical array system. For the NS component, except for the GL 0 m record, the other three records have almost the same period contents. Also, the amplitudes of the spectra do not change much with the depth. Although not shown in the figure, for the EW component, the GL 0 m record shows longer period but amplitudes for the four depths are almost the same. For UD component, liquefaction has almost no effect. The period contents for the peaks of those 4 records are within a very narrow band and spectral amplitude increases with decreasing depth.

4 DESCRIPTION OF MULTI-SHEARING MODEL

The effective stress model used in this study was proposed by Yamazaki et. al[5]. This model is composed of both deformation model with multiple non-linear

Table 1. Soil-properties used for the analysis of Port-island array

Thick. (m)	Layer Div.	ρ_t (g/cm^3)	Porosity n	K_o value	G_t*10^3 (kN/m^3)	m_v*10^{-3} (m^2/t)	ϕ' (deg.)	a	r *10^{-3}
2.0	1	1.85	0.60	0.5	53.46	-	33.0	-	-
2.0	2	1.85	0.60	0.5	53.46	-	33.0	-	-
2.0	3	1.85	0.60	0.5	81.59	1.80	34.0	0.818	2.03
2.0	4	1.85	0.60	0.5	81.59	1.80	34.0	0.818	2.03
2.0	5	1.85	0.60	0.5	81.59	1.80	34.0	0.818	2.03
2.6	6	1.85	0.60	0.5	81.59	1.80	34.0	0.818	2.03
1.4	7	1.95	0.60	0.5	86.00	1.80	34.0	0.818	2.03
2.0	8	1.95	0.60	0.5	86.00	1.80	34.0	0.818	2.03
3.0	9	1.95	0.60	0.5	86.00	1.80	34.0	0.818	2.03
2.0	10	1.65	0.40	0.5	53.46	6.00	31.5	1.000	∞
2.0	11	1.65	0.40	0.5	53.46	6.00	31.5	1.000	∞
2.0	12	1.65	0.40	0.5	53.46	6.00	31.5	1.000	∞
2.0	13	1.65	0.40	0.5	53.46	6.00	31.5	1.000	∞
1.0	14	1.95	0.35	0.6	117.05	0.90	38.0	0.818	2.03
2.0	15	1.95	0.35	0.6	117.05	0.90	38.0	0.818	2.03
2.0	16	1.95	0.35	0.6	117.05	0.90	38.0	0.818	2.03
1.0	17	1.95	0.35	0.6	117.05	0.90	38.0	0.818	2.03
4.0	18	1.95	0.35	0.6	181.40	0.90	46.0	0.715	2.73
4.0	19	1.95	0.35	0.6	181.40	0.90	46.0	0.715	2.73
4.0	20	1.95	0.35	0.6	181.40	0.90	46.0	1.000	∞
4.0	21	1.95	0.35	0.6	181.40	0.90	46.0	1.000	∞
4.0	22	2.00	0.35	0.6	245.00	0.90	48.0	1.000	∞
4.0	23	2.00	0.35	0.6	245.00	0.90	48.0	1.000	∞
4.0	24	2.00	0.35	0.6	245.00	0.90	48.0	1.000	∞
6.0	25	1.95	0.30	0.7	179.30	0.75	46.0	1.000	∞
6.0	26	1.95	0.30	0.7	179.30	0.75	46.0	1.000	∞
6.0	27	1.95	0.30	0.7	179.30	0.75	46.0	1.000	∞
4.0	28	2.00	0.30	0.7	204.80	0.90	52.0	1.000	∞

Soil constants below are adopted for all layers: permeability=10^{-6}(clay), 10^{-3}(sand) and 10^{-2}(gravel) all in m/s, failure strain=0.03, maximum damping ratio=0.35, correction factor for multi-spring=0.80, c_D=0.05

springs and pore pressure model based on strain energy concept.

The stress-strain model called the multi-spring model consists of two rigid rings and numerous non-linear springs connected together. When it represents a soil element, external forces are applied to the inner ring while the outer ring is fixed. Relation between force and deformation of each spring follows Ramberg-Osgood model with Masing rule as proposed by Ohsaki et al.[8]. For pore pressure model, it was assumed that excess pore water pressure is determined solely by accumulated shear strain energy and current values of shear stress of a soil element.

For lack of any experimental data for the site under study, the pore pressure parameters were determined using the experimental results of Toyura sand. Initial shear modulus for different soil layers were obtained from PS-logging and ϕ'values from SPT N-ϕ'relation. It was assumed that for clay layers there would be no pore pressure rise. For sand and gravel layers pore pressure parameters a and r were determined by using the relations between shear strain energy (W_s) and pore water pressure at zero shear stress (u_o) for different relative densities suggested by Towhata and Ishihara[9].

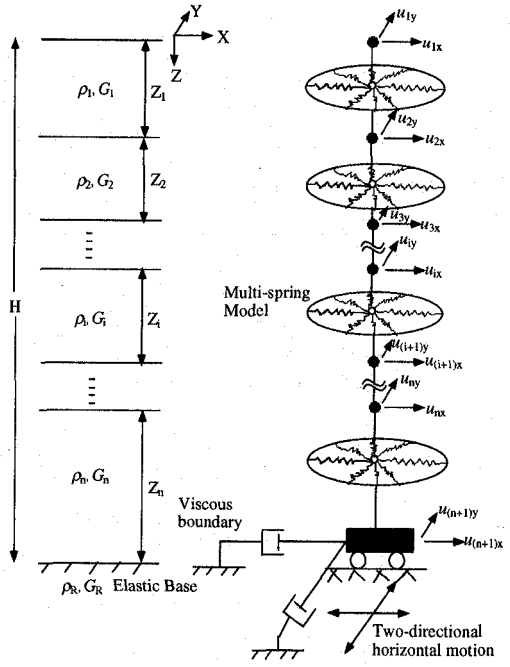

Fig.5 Model for dynamic response analysis in two-directional horizontal motion

The values of W_s and u_o obtained for a particular relative density were normalized by initial effective stress (σ'_{zo}) and put in the empirical relations suggested by Yamazaki et al.[5] to obtain parameters a and r. The empirical relations are shown below. When $u_o/\sigma'_{zo} \leq 0.5$

$$\frac{u_o}{\sigma'_{zo}} = \frac{1}{1+\left(\frac{r}{(W_s/\sigma'_{zo})}\right)^a} \qquad (1)$$

When $0.5 < u_o/\sigma'_{zo} \leq 1.0$

$$\frac{u_o}{\sigma'_{zo}} = \frac{a}{4}\left(ln(W_s/\sigma'_{zo}) - ln\, r\right) + 0.5 \qquad (2)$$

The relative density, D_r for different sands were obtained using Meyerhof[10] empirical relation shown as below,

$$D_r = 21\sqrt{\frac{N}{\sigma'_v + 0.7}} \qquad (3)$$

where, σ_V' is effective overburden pressure in kgf/cm^2. The soil parameters used for this study were shown in Table 1.

In order to carry out the integration with respect to the depth, the horizontal soil layers were divided into a number of layers. These layers were converted into a lump-mass system as shown in Figure 5 in which the masses are connected by the multi-spring model.

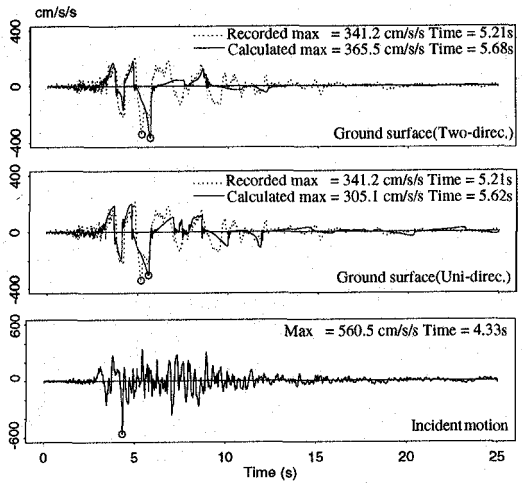

Fig.6 Computed acceleration time history (10-35s) by uni-directional and two-directional analysis for NS component

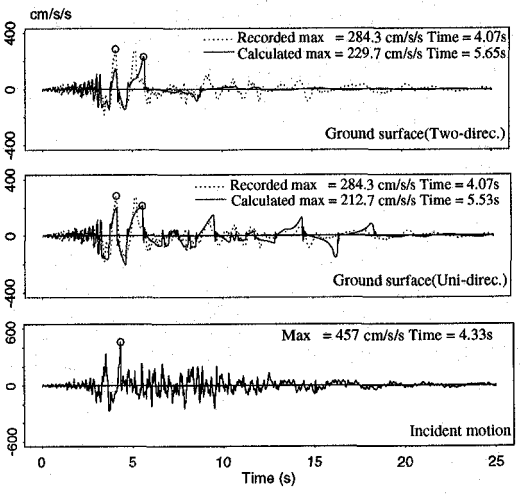

Fig.7 Computed acceleration time history (10-35s) by uni-directional and two-directional analysis for EW component

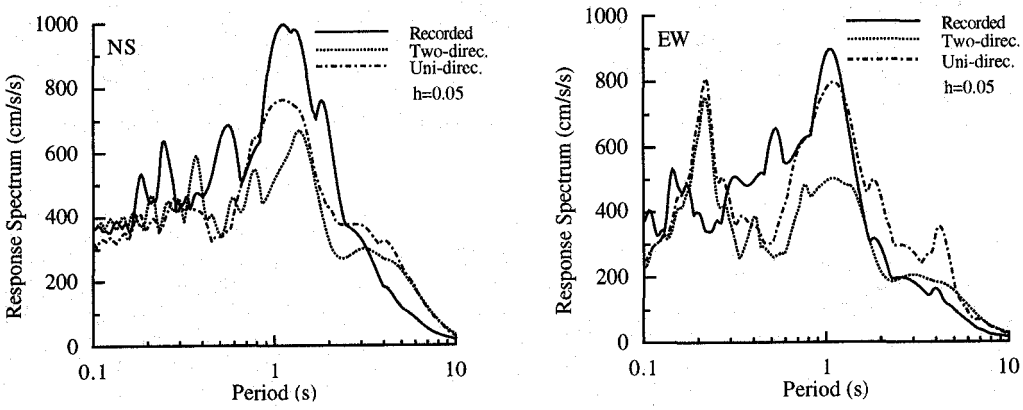

Fig.8 Computed acceleration response spectra of the ground surface for NS and EW-components

5 ANALYSIS OF THE SITE

The method of dynamic response analysis using effective stress method and multi-directional shearing for soil element was first applied for Kawagishi-cho site during the 1964 earthquake in Niigata[5,11]. For the analysis of that site the input used in the base layer were rescaled records of the earthquake observed in the basement of a building in the city of Akita. Also the site contained almost uniform soil condition, i.e., medium to fine sand. On the other hand, the site under consideration has some deep clay layers interspersed with sandy gravel layers which might have caused liquefaction at some deep layers. So, this site may be a very good opportunity to check the effectiveness of the multi-shearing model.

The acceleration records obtained in the GL-83 m in the vertical array was directly used as the incident waves. The maximum amplitudes are 560.5 cm/s^2 in NS-direction and 456.9 cm/s^2 in EW-direction. The dynamic effective stress analyses in two-directional motion and in uni-directional motion were conducted.

In general, the agreement between computed and observed results is fairly well, where as a little discrepancy in peak heights and shift of peak locations appear in some part of the time histories. Figures 6 and 7 show recorded motion at the base level (GL-83 m) and comparison between recorded motion with calculated motion on the ground surface for both two-directional and uni-directional input motions. In this figure, ground motion from 10 to 35 s are presented. The agreement appears to be very good in the region of strong shaking, the computed post-liquefaction response after 16 s are somewhat weaker than the recorded motions. This may be due to the fact that, the residual stiffness and strength assumed for the post-liquefied soil are too soft. The other factors that contribute to the discrepancy between

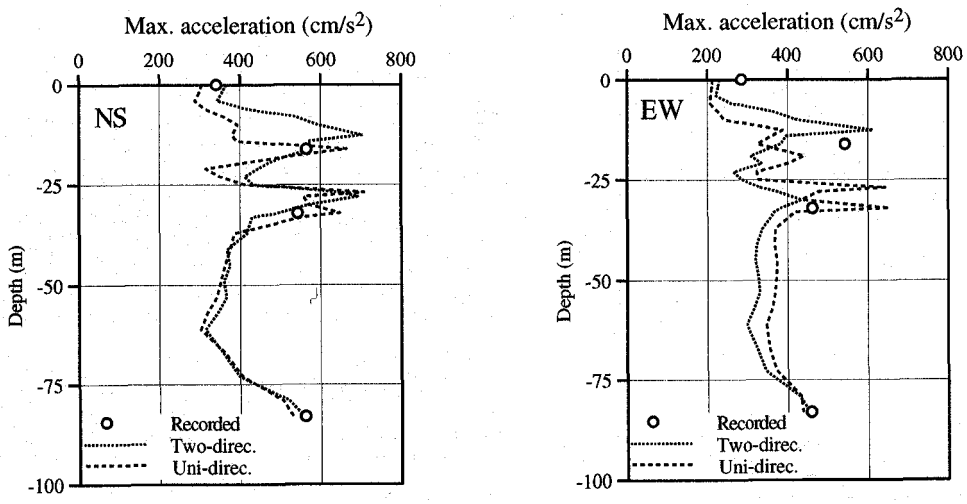

Fig.9 Distribution of the computed maximum accelerations for NS and EW-components

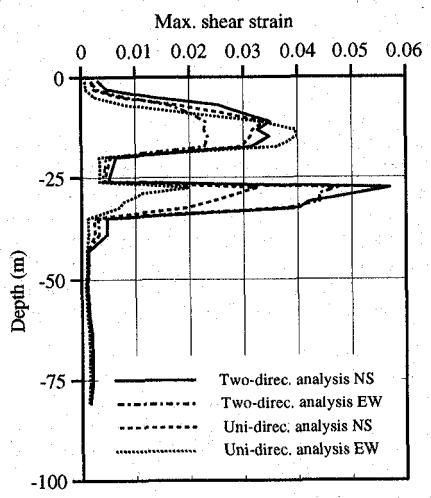

Fig.10 Distribution of the computed maximum shear strain

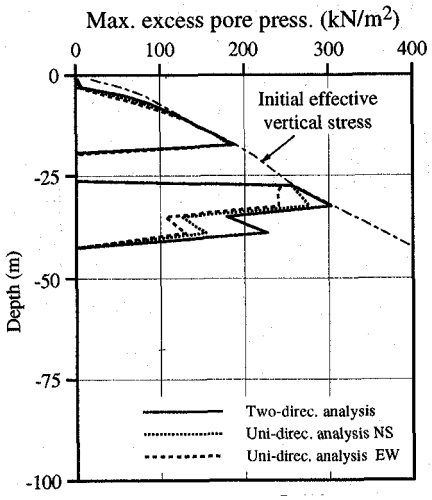

Fig.11 Distribution of the computed maximum pore-water pressure

recorded and computed motions may arise from the nature of the ground motions and the assumptions used in the 1D-analysis.

Figure 9 shows distribution of the computed maximum accelerations for NS and EW-components together with the recorded values. It can be seen that except for some top soil layers in most of the layers, maximum acceleration by two-directional analysis are smaller than the uni-directional analysis. Also from Figure 8, it can be seen that for the longer period range, spectrum values are higher for uni-directional analysis compared with the two-directional analysis. Such effects may be attributed to the fact that non-linearities of the loose layer were intensified by the combined motion.

Figures 10 and 11 show variation of maximum shear strain and maximum excess pore water pressure with depth. Figure 10 indicates possible liquified layers, as in those layers maximum strain exceed the specified failure strain. Figure 11 which shows maximum excess pore water pressure variation with depth also substantiates Figure 10.

Liquefaction may occur in more than one layer and at different times. In case of two-directional analysis, liquefaction occurred in the loose layer at GL-10 m to -16 m (i.e., layer #6 to #8) and also at GL-27 m to -33 m (layer #14 to #17). The liquefaction occurred first in the lower level and later in the upper level. The liquefaction in the lower level which occurred first can be explained by Finn et al's parametric study[12]. According to that study, if a saturated sand stratum is sealed on both sides by impermeable surfaces there will be no external drainage but an internal redistribution of pore-water pressure will take place. This will ultimately

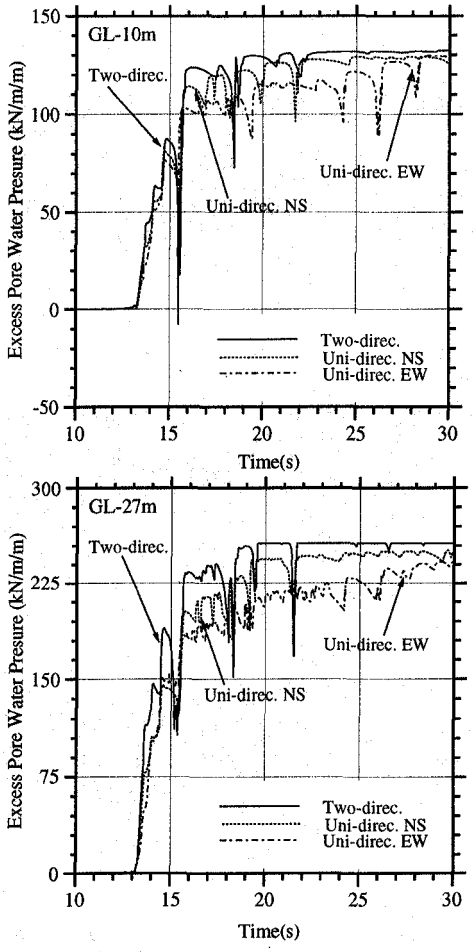

Fig. 12 Computed time histories of pore water pressures in the two liquified layers

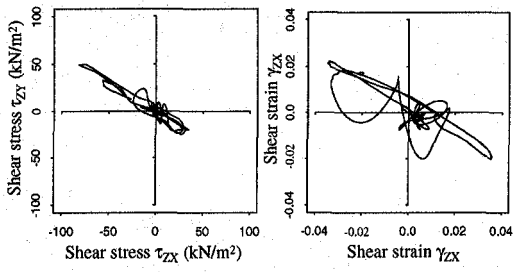

Fig. 13 Traces of shear stress and shear strain by two-directional analysis in the liquified layer at GL-10 m

raise the level of initial liquefaction and decrease the time to liquefaction within the sand layer. On the other hand, liquefaction in the upper layers which occur later can be explained by the fact that liquefaction may also occur after an earthquake ceases due to the seepage forces exerted by the upward flow of water as the pore-water pressures remaining in the soil will try to dissipate in the vertical direction. Generally, this type of liquefaction occurs near the ground surface.

In the case of uni-directional analyses the maximum pore water pressures developed in the layer #6 were 98% of the initial effective vertical stress by both NS and EW-motions. For layer #14, maximum pore water pressures developed were 93% and 98% of the initial effective vertical stress by NS and EW-motions, respectively. From Figure 12, computed time histories of pore-water pressures in two liquefied layers can be seen. The liquefaction at GL-27 m occurred before GL-10 m.

Figure 13 shows particle traces of shear stress and shear strain response at GL-10 m (#6 layer) of the soil model used for the liquefaction analysis. The particle traces show strong directivity along the same direction as the ground motion.

6 CONCLUSIONS

From the acceleration response spectra of ground motion at Kobe JMA station and Port Island site, it can be concluded that liquefaction is more prone to occur in loose or reclaimed site than in stiff site. The longer period of liquefied ground resulted due to the softening of the site by strong earthquake shaking.

Nonlinear dynamic effective stress analysis using multi-directional shearing model can well simulate the liquefaction that occurred at the Kobe Port Island array site. The results of this analysis also showed that combined two-directional input motion is more liable to cause liquefaction but induces smaller acceleration response spectrum than uni-directional input motion as observed before by Yamazaki et al.

ACKNOWLEDGEMENT

The authors would like to thank the Committee of Earthquake Observation and Research in the Kansai Area (CEORKA) for providing them with the earthquake records at the Port Island site.

REFERENCES

1. Ishihara, K. 1993. Liqefaction and flow failure during earthquakes, *Geotechnique*, **43(3)**: 351-415.
2. Seed, H.B., Pyke, R.M. & Martin, G.R. 1978. Effect of multi-directional shaking on pore pressure development in sands, *J. Geotech. Engg. Div., ASCE*, **104(GT1)**: 27-44.
3. Yamada, Y. & Ishihara, K. 1983. Undrained deformation characteristics of sand in multi-directional shear, *Soils & Foundations*, **20(1)**: 61-79.
4. Liam Finn, W.D., Ventura, C.E. & Wu, G. 1993. Analysis of ground motions at Treasure island site during the 1989 Loma Prieta earthquake, *Soil Dyn. Earth. Eng.*, **12**: 383-390.
5. Yamazaki, F., Towhata, I. & Ishihara, K. 1985. Numerical model for liquefaction problem under multi-directional shearing on horizontal plane, *Fifth Int. Conf. on Numerical Methods in Geomechanics*, Nagoya: 399-406.
6. Towhata, I. & Ishihara, K. 1985. Modelling soil behavior under principal stress axes rotation, *Fifth Int. Conf. on Numerical Methods in Geomechanics*, Nagoya: 523-530.

7. Yamazaki, F., Lu., L & Katayama, T. 1992. Orientation error estimation of buried seismographs in array obserevation, *Earth. Eng. Struct. Dyn.*, **21**: 679-694.
8. Ohsaki, Y., Hara, A. & Kiyota, Y. 1978. Stress-strain model of soils for seismic analysis, *Proc. of 5th Japan Earth. Eng. Symp.*: 697-703 (Japanese).
9. Towhata, I. & Ishihara, K. 1985. Shear work and pore water pressure in undrained shear, *Soils & Foundations*, **25(3):** 73-84.
10. Meyerhof, G.G. 1957. Discussion, Proc. *4th Int. Conf. on Soil Mechanics & Foundation Eng.*, **3**, 110.
11. Ishihara, K. & Koga, Y. 1981. Case studies of liquefaction in the 1964 Niigata earthquake, *Soils & Foundations,* **21(3):** 35-52.
12. Liam Finn, W.D., Lee, K.W & Martin, G.R. 1977. An effective stress model for liquefaction, *J. Geotech. Engg. Div., ASCE,* **103(GT6)**: 517-533.